Thin Solid Films 807 (2024) 140547

Contents lists available at ScienceDirect

Thin Solid Films

journal homepage: www.elsevier.com/locate/tsf

Structural and morphological properties of CeO_2 films deposited by radio frequency magnetron sputtering for back-end-of-line integration

Ahsan Hayat [a], Markus Ratzke [a], Carlos Alvarado Chavarin [b], Marvin H. Zoellner [b], Agnieszka Anna Corley-Wiciak [b], Markus Andreas Schubert [b], Christian Wenger [b], Inga A. Fischer [a,*]

[a] Experimentalphysik und Funktionale Materialien, Brandenburgische Technische Universität Cottbus-Senftenberg, Erich-Weinert-Straße 1, 03046, Cottbus, Germany
[b] IHP–Leibniz Institut für Innovative Mikroelektronik, Im Technologiepark 25, 15236, Frankfurt (Oder), Germany

ARTICLE INFO

Keywords:
Ceria
Hydrogen sensing
Radio-frequency sputtering
Back-end-of-line compatibility

ABSTRACT

Cerium oxides have potential applications ranging from low-temperature gas sensing to photodetection. A back-end-of-line integration of the material into complementary metal-oxide-semiconductor device fabrication processes has many advantages but places limits on material deposition, most notably the thermal budget for deposition and annealing. Here, we investigate thin cerium oxide films deposited by radio frequency (RF) magnetron sputtering at substrate temperatures of 300 °C and RF magnetron powers between 30 W and 70 W without any post-deposition annealing steps. Our investigation of the structural and morphological properties reveals a columnar texture of the thin films, and we find that the material is composed predominantly of CeO_2 (111), with a large degree of crystallinity. We discuss implications for resistive gas sensing applications.

1. Introduction

Cerium oxides are high-k dielectrics with a relative permittivity ε = 25–42 [1] and a wide bandgap between 3.2 and 3.6 eV [2] with large potential for device applications. Thin films of cerium oxides have been investigated e.g. for applications in hydrogen production [3], as functional material for photodetectors [4,5] and for applications in resistive gas sensing, where chemical interactions of the analyte gas with the sensor material lead to changes in resistivity as a measurable electrical signal. The material is chemically stable with a high diffusion coefficient for oxygen vacancies [6,7] and its potential application in gas sensing comprise oxygen [6,8,9] or hydrogen [10] detection either in its pure form [6,8] or in combination with other materials such as SnO_2 [11] or TiO_2 [9]. A tantalizing possibility is the utilization of cerium oxides in room-temperature gas sensing approaches, thus eliminating the need for sensor heating [12]. This could not only improve the energy efficiency of the sensors but also open the possibility for an integration of the material in miniaturized sensors on the complementary metal-oxide-semiconductor (CMOS) platform, e.g., for electronic nose approaches to gas sensing, with sensors and signal conditioning circuits integrated on-chip. In that context, it is interesting to consider possible back-end-of-line (BEOL) integration strategies for cerium oxides with the aim of depositing the material onto electrodes that, themselves, are fabricated in the front-end-of-line process. This, however, places requirements onto the deposition process e.g. regarding substrate temperatures, reproducibility and cost.

Deposition methods for cerium oxides that have been investigated include electron beam (e-beam) evaporation [2,13], pulsed laser deposition [14,15], atomic layer deposition [1,16] and sputtering [6,17-22]. Here, we investigate cerium oxide thin films deposited by a single radio frequency (RF) magnetron sputtering step from a cerium oxide target as a cost-effective deposition method. Compared to previous investigations, we specifically select a substrate temperature of 300 °C for deposition in order to remain within the thermal budget window required for BEOL compatibility with CMOS processing. Importantly, this requirement precludes high-temperature annealing steps, which have previously been utilized to tune material properties after sputtering [6,18-20,23]. At the same time, compared to previous investigations of cerium oxide layers sputtered at lower substrate temperatures [21,22,24], a substrate temperature of 300 °C can potentially improve layer crystallinity [17].

In cerium oxides, particle size and crystallinity have relevance for applications – the microstructure and particle size can influence gas sensing performance [25], and the growth direction has been argued to

* Corresponding author.
E-mail address: inga.fischer@b-tu.de (I.A. Fischer).

https://doi.org/10.1016/j.tsf.2024.140547
Received 6 June 2024; Received in revised form 4 October 2024; Accepted 4 October 2024
Available online 5 October 2024

impact the performance as a catalyst [26]. Given that our temperature budget is constant and limited by requirements of BEOL compatibility, we, thus, focus our investigation on the influence of the RF magnetron power on the structural and morphological properties of the cerium oxide thin films. We find that even at a substrate temperature of 300 °C, sputtering can lead to homogeneous films with good crystallinity and low surface roughness and discuss possible applications in resistive gas sensing.

2. Experimental details

Cerium oxide thin layers were deposited onto silicon (Si) (100) substrates using an RF-Magnetron Sputtering technique in a vacuum system using a 99.99 % (4 N) cerium oxide target with a diameter of 2″ as supplied by FHR Anlagenbau GmbH, Ottendorf-Okrilla, Germany. The system incorporated a water-cooled RF magnetron sputtering gun operating at 13.56 MHz, and a resistive heater was used to control the sample temperature.

The system was initially evacuated to a pressure of 10^{-4} mbar (0.01 Pa). The growth process involved using Argon (Ar) as the sputtering gas, with a continuous flow rate of 10 sccm. The substrate temperature was maintained at a fixed value of 300 °C throughout the deposition process. The RF magnetron power was varied from 30 W to 70 W with an increment of 10 W for each sample, respectively. A total of five series of experiments were carried out on 1 × 1 cm^2 substrates in this work; labelled as S1-S5 (as shown in Table 1). The distance between the target and sample was set to 4 cm for all the sputtered samples. Prior to each deposition, the target was pre-sputtered for 20 min with the closed shutter. A constant deposition time of 60 min was applied to all the samples under the study.

After deposition, the structural properties of thin films were studied using an x-ray diffraction (XRD) setup from Smart lab SE with 9 kW rotating copper anode and line focus geometry, a Ge400×2 crystal was used for monochromatization, and specular theta-2theta XRD measurements were conducted from 20–70° A Renishaw in Via system was used to collect the Raman spectra of the deposited cerium oxide layers. The spectra were obtained with a 532 nm diode laser, a grating of 2400 grooves/mm, and a 100× objective. The data was extracted from a mapping analysis at the center of the samples within an area of 25 μm^2 and a separation between spectra of ~500 nm. SEM images were taken using high-resolution scanning electron microscopy from Zeiss MERLIN Gemini 2 and the film thickness was measured by cross-sectional scanning electron microscopy (SEM) images of the cerium oxide thin film deposited on Si substrates at a SEM operating voltage of 1.5 kV. The surface morphology of the film was recorded using an atomic force microscope (AFM) in tapping mode (Dimension Icon with the Nanoscope V controller equipped with 90 μm × 90 μm × 6 μm XYZ scanner, Bruker, Billerica, MA, USA). The morphology and atomic structure of the samples were also investigated via cross-sectional images obtained from transmission electron microscopy in the scanning transmission electron microscopy (STEM) and high-resolution transmission electron microscopy (HRTEM) regimes on a Tecnai Osiris electron microscope (FEI) at the accelerating voltage of 200 kV. For HRTEM studies, the samples were prepared as transverse slices (1 1 0) using an optimized technique, including the grinding, polishing, and small-angle ion etching initially at the ion beam energies of 6 keV and then reducing the ion beam energies to 2.5 keV in the thinning stage. The digital processing of experimental HRTEM images was carried out using the commercial software package GMS-1.8 (GATAN).

Table 1
The film thicknesses of 5 different samples at different RF magnetron sputtering powers obtained from cross-sectional SEM images. The distance between the target and the sample was kept constant at 4 cm, and a working pressure of 10^{-2} mbar (1 Pa) was chosen for all samples.

Sample name	Sputtering Power (W)	Film thickness (nm)	Growth rate (nm/min)
S1	30	108.0 ± 5.4	1.80 ± 0.09
S2	40	118.5 ± 5.9	1.98 ± 0.10
S3	50	163.5 ± 8.2	2.73 ± 0.14
S4	60	218.0 ± 10.9	3.63 ± 0.18
S5	70	244.0 ± 12.2	4.07 ± 0.20

3. Results and discussion

A variation in RF magnetron power impacts the growth rate of the cerium oxide layers. We determined the growth rate for our samples based on measurements of the film thicknesses from SEM cross-sectional images for S1 - S5 (Table 1) with errors originating from a possible tilt of the cross-sectional plane of the sample in the SEM. Fig. 1 shows the relationship between sputtering power and the growth rate of deposited cerium oxide films on silicon substrates. The experimental findings demonstrate a linear correlation between growth rate and deposition power, with a slope of 0.062 nm/(min W).

The cross-sectional SEM and TEM images in combination with an AFM analysis, furthermore, confirm the presence of continuous cerium oxide films on the substrate surface. The SEM cross-sectional image clearly shows the anisotropic, columnar growth of the cerium oxide as can be seen in the Fig. 2a. This is of relevance for future applications in gas sensing, since columnar cerium oxide-based devices have been shown to possess a higher surface-to-volume ratio and a larger number of active surface sites compared to other configurations [25].

The HRTEM analysis of the cerium oxide films confirms the columnar growth morphology, as evidenced in the HRTEM micrographs (Fig. 2b, c, and, d). Moreover, an energy dispersive x-ray spectroscopy (EDX) analysis shows the homogeneous distribution of Ce and O throughout the film's thickness (Fig. 2e and f).

The surface morphology of all samples was investigated based on AFM measurements (Fig. 3). For all samples, the surface of the films is uniform and dense, with no striking differences between samples. Moreover, as evident from the AFM images, there are no defects or cracks in the sputtered films.

A more detailed investigation of the root mean square (RMS) roughness extracted from the AFM images as a function of RF power value shows an increasing trend (see Fig. 3f). In all cases, the RMS roughness was obtained from AFM scans of a 10×10 μm^2 area on the samples. Sample S3, deposited at 50 W RM magnetron power, shows a marked increase in RMS roughness, this increased roughness is present on the whole sample surface. Although deposition of all samples in the series was carried out successively within a short period of time, we cannot rule out inhomogeneities in the deposition process in our

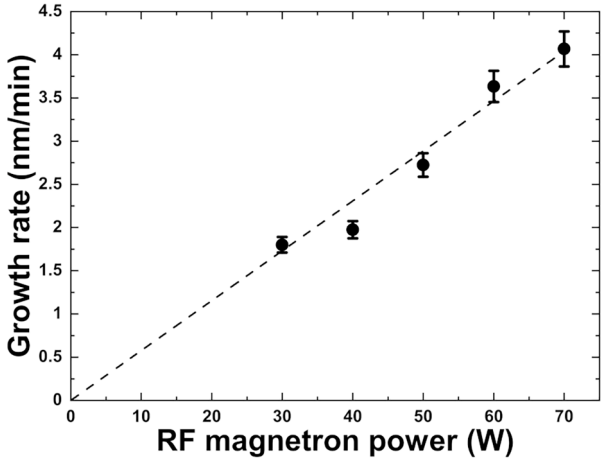

Fig. 1. The correlation between the growth rate and the RF magnetron power shows a clear linear relation.

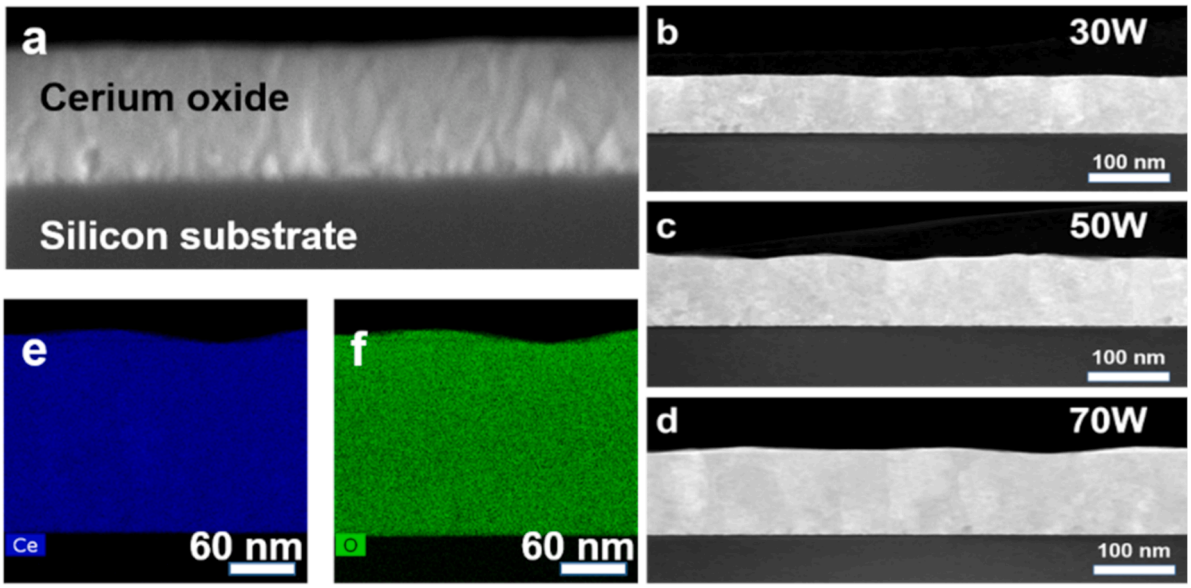

Fig. 2. (a) The SEM cross-sectional image of sample S5 (RF magnetron power of 70 W) confirms the presence of columnar growth. (b)–(d) The STEM high-angle annular dark field images of the CeO_2 films on Si substrates deposited with RF magnetron power of 30 W, 50 W, and 70 W confirm the columnar structure. (e)–(f) An EDX analysis carried out on sample S5 shows a homogeneous distribution of Ce and O.

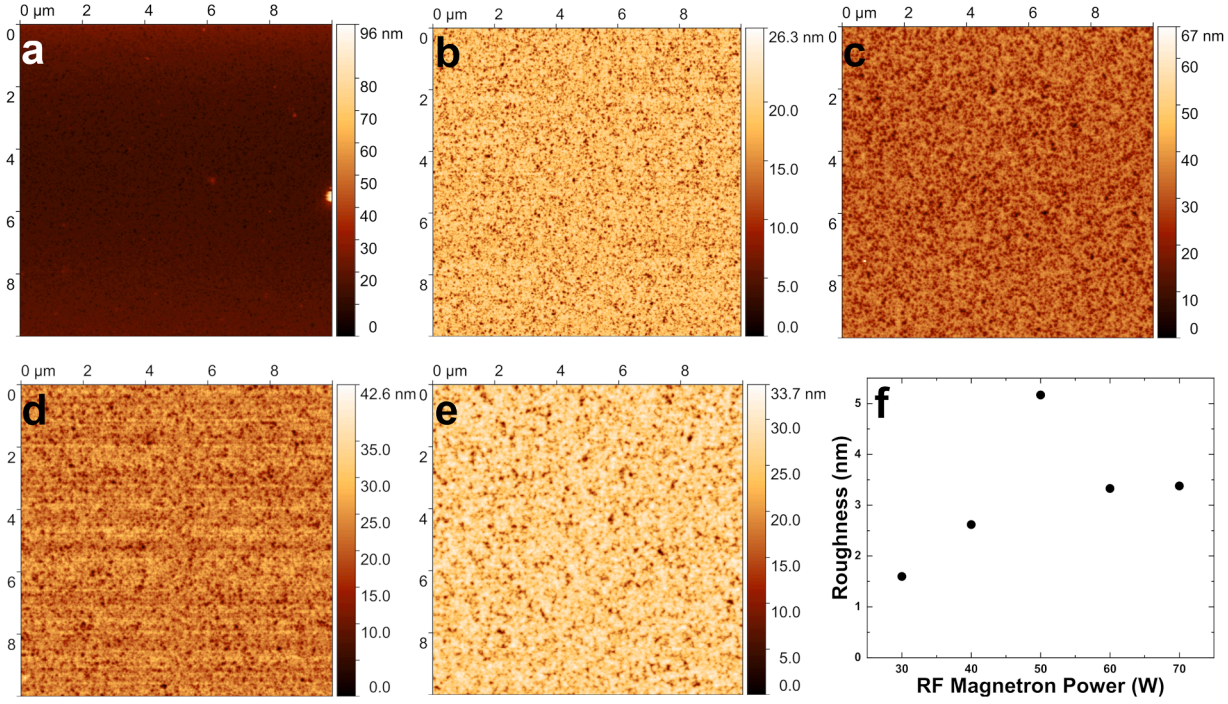

Fig. 3. The 10×10 μm^{2}AFM image of the samples S1-S5 deposited at RF magnetron power of (a) 30 W, (b) 40 W, (c) 50 W, (d) 60 W and (e) 70 W shows uniform films with no defects or cracks. (f) The root mean square (RMS) roughness values (obtained from 10×10 μm^2 areas on the samples) as a function of RF magnetron power (W) show that with an increase in RF power, the deposited films get rougher.

sputtering system, which might have contributed to the sudden increase in roughness for this sample. The general trend, i.e. an increase in roughness with increasing RF magnetron power, can be correlated with the increase in layer thickness as the RF power is increased, we also note that the divergence in thermal expansion coefficients between the cerium oxide thin film and the silicon substrate introduces the possibility of thermal stress during the film growth phase. The application of an increased deposition power might exacerbate this thermal discrepancy, potentially inducing structural disruptions within the cerium oxide film.

Cerium oxides can crystallize in different forms depending on the valence of the Ce ions: trivalent Ce^{3+} forms Ce_2O_3, whereas tetravalent Ce^{4+} forms CeO_2, the more common form of the oxides. In our sample analysis we used both Raman (Fig. 4) and XRD (Fig. 5a) characterization in order to determine the stoichiometry, crystallinity and dominant facet orientation in our Cerium oxide thin films.

In Fig. 4, the presence of the characteristic Raman peak over the whole mapping area confirms a homogeneous CeO_2 layer fully covering

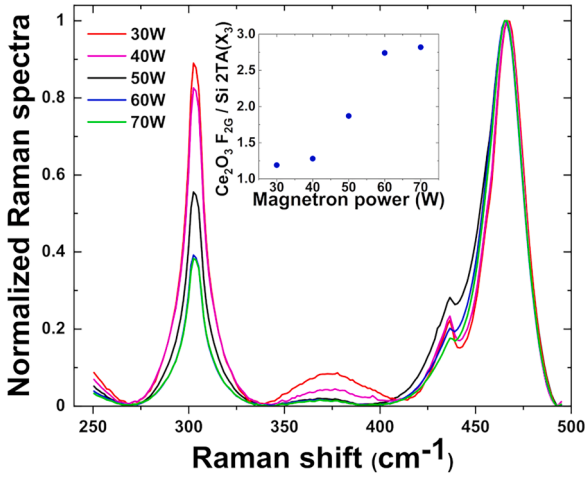

Fig. 4. Raman spectra normalized to the characteristic F2G peak of CeO_2 at different magnetron powers while maintaining constant temperature and pressure. Inset: Ratio of the F_{2G} peak to the characteristic Si peak 2TA (X_3).

the substrate. In the Raman spectra for different magnetron powers, one can observe the peaks of the Si substrate and of CeO_2. The CeO_2 exhibits a strong F_{2G} peak at 465 cm^{-1} with a full width at half maximum (FWHM) of 30 cm^{-1} [27,28]. We attribute the peak at 302 cm^{-1} with a FWHM of 40 cm^{-1} to a 2TA Si mode from the substrate and the shoulder at ~436.5 cm^{-1} to a LO Si mode, also from the substrate [29]. In our plot, the signal intensity is normalized to that of the CeO_2 F_{2G} peak. In the inset, we see a ratio of CeO_2 F_{2G} to Si 2TA peak as a function of RF magnetron power. With an increasing magnetron power, the ratio increases as the CeO_2 layer becomes thicker and eclipses the substrate.

The X-ray diffraction results are shown in Fig. 5(a). Notably, the crystal directions related to the Bragg diffraction angles (2θ) for the dominant peaks were identified as (111), (200), and (311). The CeO_2 (200) peak is only clearly visible for sample S3 (RF magnetron power of 50 W). It is also obscured by presence of the nominally basis-forbidden Si (200) peak [22] from the substrate at $2\theta = 33.2°$, which appears in the spectra of almost all samples as a consequence of multiple diffraction [30]. Nonetheless, a comparison with established reference peaks for ceria thin films and nanopowders [18,19,22] affirms the composition of the deposited material as predominantly CeO_2. Our samples exhibit clear CeO_2 (111) peaks independently of RF magnetron power, indicating that the preferred crystallite orientation is along the (111) direction. Different deposition methods have been reported to influence the preferred crystallite orientation of CeO_2 on Silicon (100) substrates, with a (110) preferred orientation obtained from e-beam evaporation [31], for example. The (111) direction of CeO_2 structure is energetically the most stable one [26], and has previously found to be the preferred crystallite orientation for RF magnetron sputtered films at low substrate temperatures [18,19]. While thin films are generally more likely to have a crystal orientation corresponding to that of the substrate at lower deposition rates, we nonetheless find the (111) facet to be the most frequently exposed one in our thin films irrespective of the deposition rate.

Finally, we also investigated the average crystallite size as a function of magnetron power for the sample series (Fig. 5b). The weighted average crystallite size was determined by extracting the full width at half maximum (FWHM) for the (111) diffraction peaks using results obtained from the Pearson VII fitting model in Origin for each sample. We determined the crystallite sizes d_p using Debye's Scherer equation

$$d_p = \frac{0.9\ \lambda}{B\ cos\theta},$$

where, λ, B, and θ are the X-ray wavelength ($\lambda = 1.54$ Å), FWHM of the CeO_2 (111) diffraction peak, and Bragg diffraction angle, respectively. In our investigation, we found only a very weak increase of the crystallite sizes with increasing RF magnetron power. The average crystallite sizes between 16 and 19 nm in our samples are only slightly larger than crystallites obtained from RF magnetron sputtering at room temperature, where values between 12 and 18 nm have been reported [22]. Crystallite sizes influence gas sensor response times, where faster response times can be expected for smaller crystallites [32].

4. Conclusion

Previous investigations concerning sputtered cerium oxide films have often focussed on utilizing elevated substrate temperatures during deposition or on the use of high-temperature annealing steps after deposition in order to achieve films with desired properties [6,20]. Here, our investigation targets structural and morphological properties of sputtered Cerium oxide for possible applications in BEOL device fabrication. As such, we keep the substrate temperature fixed at 300 °C during deposition and only vary the RF magnetron power. We find that even at this moderate substrate temperature during deposition, our sputtered films contain CeO_2 with a large degree of crystallinity and well-defined facet orientation irrespective of RF sputtering power. Cross-sectional images of our sputtered films exhibit a columnar texture, which has previously been shown to be advantageous for gas sensing applications [25]. The surface roughness of our films increases with increasing film thickness but is low for all deposition parameters

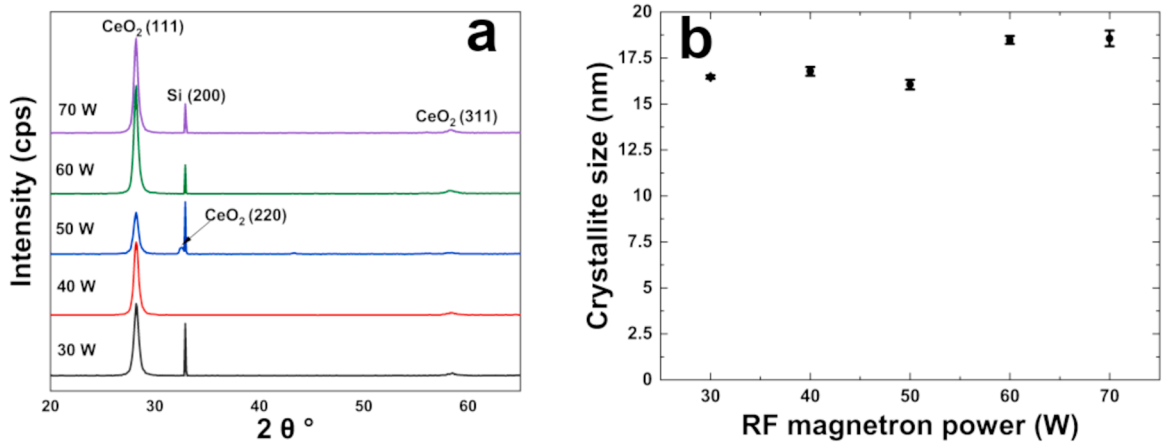

Fig. 5. (a) XRD diffraction patterns for all samples. (b) A plot of average crystallite sizes versus magnetron power for the sample series shows a very weak trend towards larger crystallite sizes with increasing RF magnetron power.

investigated here. We obtain small CeO_2 crystallites with diameters below 20 nm, which can be expected to be advantageous for sensor response times [32].

The structural and morphological properties of our sputtered CeO_2 films, thus, show promise for gas sensing applications, which will be the subject of future work. Future investigations can focus on utilizing CeO_2 layers deposited at RF magnetron power of 70 W, i.e. with the largest growth rate, which is advantageous from a fabrication point of view. While the surface area of our sputtered films is reduced in our continuous films compared to porous CeO_2 films or nanoparticle layers obtained by other deposition methods, the reproducibility of our method nonetheless poses considerable advantages for applications of the material in BEOL sensor fabrication. This could pave the way for large-scale fabrication of CeO_2-based gas sensors on the cost-effective Si platform.

CRediT authorship contribution statement

Ahsan Hayat: Writing – original draft, Investigation, Formal analysis, Data curation. **Markus Ratzke:** Writing – review & editing, Investigation, Formal analysis. **Carlos Alvarado Chavarin:** Writing – review & editing, Investigation, Formal analysis, Data curation, Conceptualization. **Marvin H. Zoellner:** Writing – review & editing, Investigation, Formal analysis. **Agnieszka Anna Corley-Wiciak:** Writing – review & editing, Investigation. **Markus Andreas Schubert:** Writing – review & editing, Investigation, Formal analysis. **Christian Wenger:** Writing – review & editing, Supervision, Funding acquisition. **Inga A. Fischer:** Writing – original draft, Supervision, Resources, Project administration, Funding acquisition, Formal analysis, Data curation, Conceptualization.

Declaration of competing interest

The authors declare the following financial interests/personal relationships which may be considered as potential competing interests:

Inga Fischer reports financial support was provided by Federal Ministry of Education and Research Bonn Office. If there are other authors, they declare that they have no known competing financial interests or personal relationships that could have appeared to influence the work reported in this paper.

Data availability

Data will be made available on request.

Acknowledgements

The authors would like to thank the financial support by the Federal Ministry of Education and Research of Germany under grant numbers 16ES1131 and 16ES1128K.

References

[1] P.J. King, M. Werner, P.R. Chalker, A.C. Jones, H.C. Aspinall, J. Basca, J.S. Wrench, K. Black, H.O. Davies, P.N. Heys, Effect of deposition temperature on the properties of CeO_2 films grown by Atomic Layer Deposition, Thin Solid Films 519 (2011) 4192–4195, https://doi.org/10.1016/j.tsf.2011.02.025.

[2] C. Mansilla, Structure, microstructure and optical properties of cerium oxide thin films prepared by electron beam evaporation assisted with ion beams, Solid. State Sci. 11 (2009) 1456–1464, https://doi.org/10.1016/j.solidstatesciences.2009.05.001.

[3] J. Kugai, S. Velu, C. Song, Low-temperature reforming of ethanol over CeO_2-supported Ni-Rh bimetallic catalysts for hydrogen production, Catal. Letters. 101 (2005) 255–264, https://doi.org/10.1007/s10562-005-4901-7.

[4] N.V. Maksimchuk, A.V. Borisov, Nanocrystalline cerium oxide films as a functional material for photodetectors of bioluminescent signal, in: Proceedings of the 2013 IEEE XXXIII International Scientific Conference Electronics and Nanotechnology, 2013, pp. 205–207, https://doi.org/10.1109/ELNANO.2013.6552034.

[5] S. Zinzuvadiya, N.C. Pandya, U.S. Joshi, Optoelectronic response of (111) oriented CeO_2 films for UV photodetector, Thin Solid Films 669 (2019) 525–530, https://doi.org/10.1016/j.tsf.2018.11.055.

[6] J. Gerblinger, W. Lohwasser, U. Lampe, H. Meixner, High temperature oxygen sensor based on sputtered cerium oxide, Sens. Actuators B Chem. 26 (1995) 93–96, https://doi.org/10.1016/0925-4005(94)01564-x.

[7] L. Pîslaru-Dănescu, G. Telipan, I. Ion, V. Marinescu, Prototyping a Gas Sensors Using CeO_2 As a Matrix or Dopant in Oxide Semiconductor Systems, Cerium Oxide-Applications and Attributes, IntechOpen, 2018, https://doi.org/10.5772/intechopen.80801.

[8] N. Ramshanker, K.L. Ganapathi, M.S. Bhat, RF Sputtered CeO_2 thin films-based oxygen sensors, IEEe Sens. J. 19 (2019) 10821–10828, https://doi.org/10.1109/JSEN.2019.2931766.

[9] A. Trinchi, Y.X. Li, W. Wlodarski, S. Kaciulis, L. Pandolfi, S. Viticoli, E. Comini, G. Sberveglieri, Investigation of sol–gel prepared CeO_2–TiO_2 thin films for oxygen gas sensing, Sens. Actuators B Chem. 95 (2003) 145–150, https://doi.org/10.1016/s0925-4005(03)00424-6.

[10] K. Suzuki, H. Miyazaki, Y. Yuzuriha, Y. Maru, N. Izu, Characterization of a novel gas sensor using sintered Ceria nanoparticles for hydrogen detection in vacuum conditions, Sens. Actuators B Chem. 250 (2017) 617–622, https://doi.org/10.1016/j.snb.2017.05.008.

[11] P. Chesler, C. Hornoiu, V. Bratan, C. Munteanu, G. Postole, N.I. Ionescu, T. Juzsakova, A. Redey, M. Gartner, CO sensing properties of SnO_2–CeO_2 mixed oxides, React. Kinet. Mech. Catal. 117 (2015) 551–563, https://doi.org/10.1007/s11144-015-0970-9.

[12] M.A. Takte, N.N. Ingle, B.N. Dole, M.-L. Tsai, T. Hianik, M.D. Shirsat, A stable and highly-sensitive flexible gas sensor based on Ceria (CeO_2) nano-cube decorated RGO nanosheets for selective detection of NO_2 at room temperature, Synth. Met. 297 (2023) 117411, https://doi.org/10.1016/j.synthmet.2023.117411.

[13] T. Wiktorczyk, P. Biegański, E. Zielony, Preparation and optical characterization of e-beam deposited cerium oxide films, Opt. Mater. (Amst) 34 (2012) 2101–2107, https://doi.org/10.1016/j.optmat.2012.05.027.

[14] D. Kek-Merl, J. Lappalainen, H.L. Tuller, Electrical properties of nanocrystalline CeO_2 thin films deposited by in situ pulsed laser deposition, J. Electrochem. Soc. 153 (2006) 15, https://doi.org/10.1149/1.2165778.

[15] G. Balakrishnan, S.T. Sundari, P. Kuppusami, P.C. Mohan, M.P. Srinivasan, E. Mohandas, V. Ganesan, D. Sastikumar, A study of microstructural and optical properties of nanocrystalline Ceria Thin films prepared by pulsed laser deposition, Thin Solid Films 519 (2011) 2520–2526, https://doi.org/10.1016/j.tsf.2010.12.013.

[16] S. Vangelista, R. Piagge, S. Ek, T. Sarnet, G. Ghidini, C. Martella, A. Lamperti, Structural, chemical and optical properties of cerium dioxide film prepared by atomic layer deposition on tin and Si substrates, Thin Solid Films 636 (2017) 78–84, https://doi.org/10.1016/j.tsf.2017.05.034.

[17] S. Yaegashi, T. Kurihara, H.H. Hideo Hoshi, H.S. Hideo Segawa, Epitaxial growth of CeO_2 films on Si (111) by sputtering, Jpn. J. Appl. Phys. 33 (1994) 270, https://doi.org/10.1143/JJAP.33.270.

[18] L. Kim, J. Kim, D. Jung, C.-Y. Park, C.-W. Yang, Y. Roh, Effects of deposition parameters on the crystallinity of CeO_2 thin films deposited on Si (100) substrates by R.F.-magnetron sputtering, Thin Solid Films 360 (2000) 154–158, https://doi.org/10.1016/s0040-6090(99)01087-1.

[19] N. Muslim, M.N.S.I.M. Idris, Y.W. Soon, N.Y. Voo, A Study on the surface of RF magnetron sputtered CeO_2 thin films at relatively low substrate temperature, IOP Conf. Ser. Mater. Sci. Eng. 538 (2019) 012019, https://doi.org/10.1088/1757-899X/538/1/012019.

[20] H.-Y. Lee, Y.-C. Lee, Y.-P. Hong, K.-H. Ko, Interfacial reactions between RF sputtered CeO_2 film and Si (100) substrate, Appl. Surf. Sci. 228 (2004) 164–168, https://doi.org/10.1016/j.apsusc.2004.01.005.

[21] R. Murugan, G. Vijayaprasath, P. Sakthivel, T. Mahalingam, G. Ravi, Structural, morphological and optical properties of CeO_2 thin films deposited by RF Sputtering, AIP. Conf. Proc. (2016) 80029, https://doi.org/10.1063/1.4947907.

[22] P.-C. Chen, X.A. Wang, Cerium oxide film growth using radio-frequency sputtering process, Mater. Sci. Appl. 11 (2020) 305–318, https://doi.org/10.4236/msa.2020.115021.

[23] A. Eltayeb, R.K. Vijayaraghavan, A.P. McCoy, J. Cullen, S. Daniels, E. McGlynn, Control of crystal structure, morphology and optical properties of Ceria films by post deposition annealing treatments, Thin Solid Films 603 (2016) 363–370, https://doi.org/10.1016/j.tsf.2016.02.036.

[24] R. Murugan, G. Vijayaprasath, T. Mahalingam, Y. Hayakawa, G. Ravi, Effect of rf power on the properties of magnetron sputtered CeO_2 thin films, J. Mater. Sci. Mater. Electron. 26 (2015) 2800–2809, https://doi.org/10.1007/s10854-015-2761-5.

[25] D. Barreca, A. Gasparotto, C. Maccato, C. Maragno, E. Tondello, E. Comini, G. Sberveglieri, Columnar CeO_2 nanostructures for sensor application, Nanotechnology. 18 (2007) 125502, https://doi.org/10.1088/0957-4484/18/12/125502.

[26] I. Zumeta-Dubé, J.M. García Rangel, J. Roque, I.C. Romero-Ibarra, M.F. García Sánchez, Strong texture tuning along different crystalline directions in glass-supported CeO_2 thin films by ultrasonic spray pyrolysis, Sci. Rep. 11 (2021), https://doi.org/10.1038/s41598-021-81353-x.

[27] W.H. Weber, K.C. Hass, J.R. McBride, Raman study of CeO_2: second-order scattering, lattice dynamics, and particle-size effects, Phys. Rev. B 48 (1993) 178–185, https://doi.org/10.1103/physrevb.48.178.

[28] C. Schilling, A. Hofmann, C. Hess, M.V. Ganduglia-Pirovano, Raman spectra of polycrystalline CeO_2: A density functional theory study, J. Phys. Chem. C 121 (2017) 20834–20849, https://doi.org/10.1021/acs.jpcc.7b06643.

[29] I. Iatsunskyi, S. Jurga, V. Smyntyna, M. Pavlenko, V. Myndrul, A. Zaleska, Raman spectroscopy of nanostructured silicon fabricated by metal-assisted Chemical Etching, Optical Micro- and Nanometrology V. (2014) 323–329. doi:10.1117/12.2051489.

[30] P. Zaumseil, High-resolution characterization of the forbidden Si 200 and Si 222 reflections, J. Appl. Crystallogr. 48 (2015) 528–532, https://doi.org/10.1107/s1600576715004732.

[31] T. Inoue, T. Ohsuna, L. Luo, X.D. Wu, C.J. Maggiore, Y. Yamamoto, Y. Sakurai, J. H. Chang, Growth of (110)-oriented CeO_2 layers on (100) silicon substrates, Appl. Phys. Lett. 59 (1991) 3604–3606, https://doi.org/10.1063/1.105646.

[32] N. Izu, W. Shin, I. Matsubara, N. Murayama, The effects of the particle size and crystallite size on the response time for resistive oxygen gas sensor using cerium oxide thick film, Sens. Actuators B Chem. 94 (2003) 222–227, https://doi.org/10.1016/s0925-4005(03)00330-7.